Thrust Performace Assessment of Sub-scale Magnetic Sails by Particle Method

Kazuhisa FUJITA*

Abstract : Electromagnetic interaction between the solar wind and sub-scale magnetic sails was numerically analyzed to assess reaction forces exerted on the magnetic sail when its characteristic scale is reduced below the continuum limit at which the magneto-hydrodynamic approximations for the plasma flow fail. The hybrid particle-in-cell (PIC) method was used to take the finite Larmor-radius effects into consideration. The magnetic dipole intensity was changed so that the characteristic size of the magnetic sail changed from several kilometers to few thousand kilometers. The results show that the drag coefficient of the magnetic sail based on the representative radius of the magneto-hydrodynamic interaction decreases as the ratio of the ion Larmor radius to this representative radius becomes greater than unity. An approximate formula to compute the drag coefficient in a wide range of magnetic sail dimension has been developed.

Introduction

The primary barriers to deep space explorations may be low thrust densities, low thrust efficiencies, low specific impulses, or low thrust-to-power ratios of existing space propulsion systems. Although ion engines can actualize high specific impulses, their thrust densities are so low that long flight time to the target planet is inevitable. Contrary to this, the chemical propulsion can realize only poor specific impulses in exchange for high thrust densities to accelerate a spacecraft quickly. In order to increase a chance for low-cost, frequent, and quick access to deep space explorations, a breakthrough in space propulsion technologies may be necessary. From this viewpoint, as one of candidates for advanced space propulsion, solar sails and magnetic sails were studied in the past. Although their specific impulses are infinite in principal, there is an essential problem from an engineering standpoint that unrealistically gigantic structures should be constructed or deployed, and kept under control during the flight. For this reason, researches of the solar and the magnetic sails have slowed down.

Recently, Winglee and his coworkers have proposed an idea of magnetic inflation, in which the initial magnetic field attached to a spacecraft is expanded by injection of high-beta plasmas from the spacecraft to form finally a huge magnetic field, namely a magnetoplasma-sail (MPS), in place of using a substantial conducting coil of great dimensions[1-3]. In view of reduced difficulty in producing a gigantic magnetic field, interests in using the solar wind for interplanetary propulsion have been renewed. Following Winglee, the author and coworkers have started to assess the feasibility of this concept, using both theoretical and experimental approaches[4-9].

In principle, both the magnetic sails and the magnetoplasma sails are accelerated by the Lorentz force originating

* IAT/JAXA

from interaction between the electric current induced in the solar wind plasma and the magnetic dipole in the spacecraft. Like in the electromagnetic interaction between the terrestrial magnetic dipole and the solar wind, in a quasi-steady state, the magnetic field generated by the spacecraft is surrounded by the magnetosphere boundaries, beyond which the solar wind plasmas cannot penetrate directly into the magnetosphere. Thrust obtainable from the solar wind is expected to be proportional to the cross section of the magnetosphere with respect to the stream direction, just like an aerodynamic drag about a blunt-body object in the atmospheric hypersonic flight. In such a situation, momentum of the solar wind is equilibrated with the magnetic pressure on the magnetosphere boundary, resulting in a unique magnetic flux density of $B \approx 40$ nT just inside this boundary. Larmor radii for electrons and protons for this magnetic flux density are at the order of 100 m and 100 km, respectively.

In practical applications, the dimension of the magnetosphere may be limited due to engineering implementabilities such as the induction coil and the power resources. With respect to the MPS, the dimension of the magnetosphere may be subject to the efficiency of magnetic field inflation in addition. If the representative radius of the magnetosphere is smaller than the ion Larmor radius, acceleration forces predicted by magneto-hydrodynamic (MHD) models may suffer from considerable errors, since MHD models are based on an assumption that Larmor radii of both electrons and ions are infinitely small in relation to the representative scales of the magnetic field.

Such a problem is known as the finite Larmor-radius effect in the field of nuclear fusion technologies and planetary plasma simulations. However, how the finite Larmor radius exerts an influence on acceleration force of the magnetic sail has not been well understood. In the past study[9], to gain primary understandings of acceleration force generation in dipolar magnetic fields, electromagnetic interactions between sub-scale magnetic fields and plasma flows were numerically simulated by the full particle-in-cell (PIC) method in which kinetic motions of both electrons and ions are computed, using a magnetic field of small dimension. More practically, to perform a quantitative assessment of the finite Larmor-radius effect on acceleration force generation in moderately-scaled magnetic sails, the hypersonic plasma flows around the magnetic field are solved by the hybrid PIC method in this article.

Method of Analysis

Particle-in-Cell Model

The plasma flows and the electromagnetic fields are numerically computed by the hybrid PIC method. In this approach, electrons are treated as a continuum fluid consisting of massless particles, while kinetic motion of ions is solved in terms of sample particles. Since details of the hybrid PIC method can be found in the literature (Ref.10 , for example), only a brief description is given below. As a primary assumption, the hypersonic plasma flows are assumed to consist of electrons and protons without Coulomb collisions, since the solar wind is highly rarefied. Kinetic motion of each proton is expressed by the equations of motion as

$$\frac{\partial \boldsymbol{v}_i}{\partial t} = \frac{e}{m_i}(\boldsymbol{E} + \boldsymbol{v}_i \times \boldsymbol{B}) \tag{1}$$

$$\frac{\partial \boldsymbol{r}_i}{\partial t} = \boldsymbol{v}_i \tag{2}$$

where $\boldsymbol{r}_i$ and $\boldsymbol{v}_i$ are the position and the velocity vectors of a proton, e is the elementary charge, m_i is the mass of a proton, and $\boldsymbol{E}$ and $\boldsymbol{B}$ are the electric field and the magnetic flux density vectors, respectively. The momentum

conservation for the electron fluid is approximated by

$$en_e(\boldsymbol{E}+\boldsymbol{V}_e\times\boldsymbol{B})+\nabla p_e=0 \tag{3}$$

where n_e is the number density of electrons, V_e is the mean velocity vector of the electron fluid, and p_e is the electron pressure. Electrical neutrality is assumed by

$$n_e=n_i \tag{4}$$

where n_i is the number density of ions.

In this analysis, motion of the electron fluid is assumed to be isentropic since the electron fluid is subsonic everywhere in the flow under consideration, and since no external electric field is imposed. Consequently, the equation for electron energy conservation is not solved but an isentropic relation between the pressure and the density is introduced as

$$p_e/n_e^{\gamma}=\text{const.} \tag{5}$$

where γ is the specific heat ratio for the electron fluid.

Maxwell's equations describing the electromagnetic field are reduced based on the Darwin approximation, as

$$\frac{\partial \boldsymbol{B}}{\partial t}=-\nabla\times\boldsymbol{E} \tag{6}$$

$$\boldsymbol{j}=\frac{1}{\mu_0}\nabla\times\boldsymbol{B}=e(n_i\boldsymbol{V}_i-n_e\boldsymbol{V}_e) \tag{7}$$

where μ_0 is the magnetic permeability of vacuum and V_i is the mean velocity vector of protons. Combination of Eqs.(3),(4), and (7) with elimination of n_e and V_e yields an explicit expression for the electric field as

$$\boldsymbol{E}=\left(\frac{1}{en_i\mu_0}\nabla\times\boldsymbol{B}\right)\times\boldsymbol{B}-\boldsymbol{V}_i\times\boldsymbol{B}-\frac{1}{en_i}\nabla p_e \tag{8}$$

Equations (3) and (7) fail when particle densities are zero in the absence of a sample particle. In such a situation, the electric field is determined alternatively by

$$\nabla\cdot\boldsymbol{E}=0 \text{ and } \boldsymbol{E}=-\nabla\phi \tag{9}$$

where ϕ is the electrostatic potential. Equation(6) is reduced to

$$\frac{\partial \boldsymbol{B}}{\partial t}=0 \tag{10}$$

since $\nabla\times\nabla\phi=0$.

Numerical Procedure

To perform the particle simulation with statistical operation involved, the electromagnetic field solvers are incorporated into the multi-purpose DSMC code, RARAC-3D[11]. Equations (1) and (2) are integrated in time by the 4th-order Runge-Kutta method for each sample particle. The average density and the average velocity, n_i and V_i respectively, are determined at each computational node from positions of sample particles by linear weighting (PIC method). The electron pressure is calculated by Eqs.(4) and (5) from the average ion density. The magnetic field is then determined by Eq.(6) from the electric and the magnetic field at the previous time step, and the electric field is

Table 1: Scale parameters for magnetic sail and computational domain.

Case	$\mu_0 m/4\pi$ (Tm^3)	r_0(m)	r_1(m)	R_L	r_c/r_0	r_L/r_0	r_1/r_0	δ/r_0[b]
1	4.34^{+10}[a]	3.16^{+05}	3.08^{+06}	0.100	3.22	10.2	9.73	0.323
2	1.37^{+09}	1.00^{+05}	9.73^{+05}	0.316	3.22	5.73	9.73	1.02
3	4.34^{+07}	3.16^{+04}	3.08^{+05}	1.00	3.22	3.22	9.73	3.23
4	1.37^{+06}	5.62^{+03}	5.47^{+04}	3.16	5.73	3.22	9.73	18.2
5	4.34^{+04}	1.00^{+03}	1.38^{+04}	10.0	10.2	3.22	9.73	102

[a] 4.34^{+10} stands for 4.34×10^{10}, for example.
[b] $\delta = 1.02\times10^5$(m) is the skin depth of the solar wind plasma.

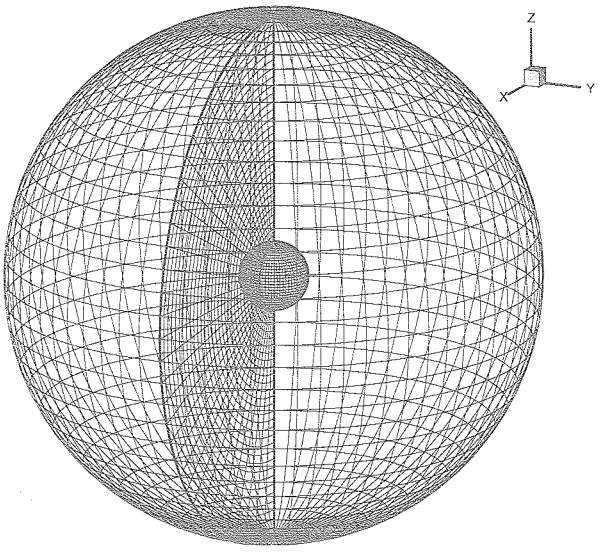

Fig 1: Spherical grid system consisting of 30-radial × 37-latitudinal × 73-longitudinal nodes.

etermined finally by Eq.(8) or (9).

In order to enhance accuracy in time integration, the leapfrog technique[10] is used by introducing half-integral time steps. Since the magnetic flux density generated by a magnetic dipole varies roughly in proportion to r^{-3}, fine grids are necessary in the region where r is small for the flow and the magnetic filed to be solved accurately. To realize this, a spherical grid system with radial reticulation is used in this study. The magnetic dipole is placed at the origin of the spherical grid system, aligned with the z coordinate in the positive direction. In order to avoid an excessive increase of the magnetic field intensity in the calculation domain, the inner boundary is set at $r = r_0$, which is small enough to have no influence on the flow and the magnetic field in electromagnetic interaction. The magnetic field intensity is fixed during time integration on this inner boundary. On the other hand, the outer boundary is set at $r = r_1$, depending on the magnetic dipole intensity, so that the final results are not affected by this boundary. A typical example of the grid system is shown in Fig.1. In addition to this base grid system, a staggered grid system is introduced to maintain $\nabla \cdot B = 0$ precisely during time integration. The magnetic filed are defined at the staggered grid system.

Solar Wind and Magnetic Dipole Models

The solar wind is assumed to be a hypersonic plasma flow consisting of electrons and protons. Protons are assumed to be members of a Maxwell-Boltzmann velocity distribution function at 0.3 eV, while the electron temperature is assumed to be 10 eV. Average flow velocities of both electrons and protons are set identically to be 400 km/s. Average number densities of electrons and protons are given uniquely as 5×10^6 m^{-3}, based on the representative value at 1 A.U. The interplanetary magnetic field in the solar wind is neglected in this study. Proton samples are added at every outer surface element of the computational domain by the statistical inflow conditions based on the Boltzmann velocity distribution and the flow velocity. The flow direction is aligned to the x coordinate in the negative direction.

One important scaling parameter is the distance from the dipole center at which the dynamic pressure of the solar wind is equilibrated with the magnetic pressure produced by the initial magnetic field. This distance, denoted hereafter by r_c, represents the radius of the magnetic sail with respect to magneto-hydrodynamic interaction against the solar wind in a MHD approximation. Another scaling parameter is the distance from the dipole center at which the ion Larmor radius, L_i, is locally equivalent to the distance from the dipole center. This distance, defined by r_L, is the radius of the magnetic sail with respect to particulate Lorentzian interaction, in which motion of each proton is controlled by Lorentz force due to the initial magnetic field of the magnetic dipole. The ratio of L_i at $r = r_c$ to r_c, defined hereafter by $R_L \equiv L_i(r_c) / r_c$, is an important non-dimensional parameter representing the finite Larmor-radius effect in the magneto-hydrodynamic interaction. In the series of comparative computations, the value of R_L is changed by changing the magnetic dipole intensity, m.

The scale parameters of the magnetic sail and the computational domain are summarized in Table1. Dimension of the computational domain is changed in accordance with a variation of R_L so that the representative interaction radius, r_c or r_L depending on $R_L < 1$ or $R_L \geq 1$ respectively, can be located between $r = 3r_0$ and $6r_0$ in an attempt to reduce influences of grid resolution on the computed reaction force exerted on the magnetic dipole (see sixth and seventh column in Table1). Values of R_L ranging from 0.1 to 10.0 are tested in this study, which corresponds to variation of r_c from 10.2 to 3220 km. In the present study, the reaction force is calculated from a change in net kinetic momentum of inflowing and outflowing sample particles.

Numerical Results

Distribution of sample particles and magnetic field lines around the magnetic dipole for several computation cases are shown in Fig.2. Although the flow and the magnetic fields shown in Fig.2 are in a quasi-steady state statistically, instantaneous views of the flow and the magnetic fields suffer from slight fluctuations since they are essentially nonstationary in particle simulations. When the finite Larmor-radius effect is small ($R_L < 1$), magnetic field lines are deflected toward downstream due to induced current generated in the solar wind plasma. In this case, interaction between the solar wind and the magnetic field around the dipole is close to that predicted using the MHD approximations, since the Larmor radius at the magnetosphere boundary is much smaller than dimension of the magnetosphere. In Case 1, the skin depth of the solar wind is expected to be 0.323 r_0, as shown in Table1. In Fig.2a, the magnetic field lines do not seem to penetrate into the solar wind plasma, resulting in a distinct magnetosphere boundary around the magnetic dipole. An ion acoustic shock wave and a shock layer are formed ahead of the magnetosphere, as shown in Fig. 3a.

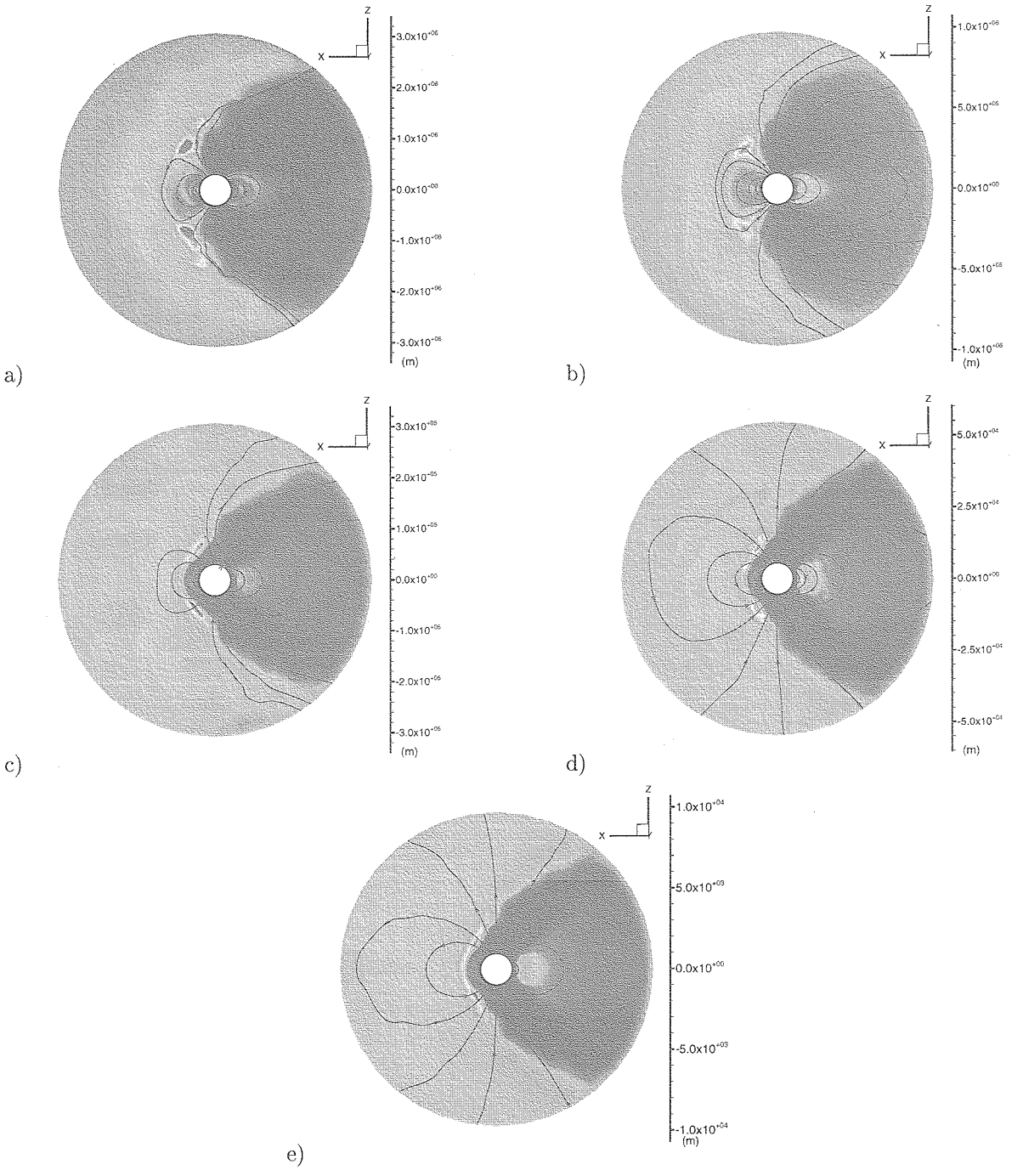

Fig 2: Distributions of sample particles and magnetic field lines on $x - z$ plane for a) $R_L = 0.100$, b) 0.316, c) 1.00, d) 3.16, and e) 10.0.

In contrast to this, as R_L increases or the ratio of δ to r_c increases, the magnetic field lines become less deflected toward downstream and penetrate into the solar wind plasma to a greater extent, resulting in a less distinct magnetosphere boundary, as seen in Figs. 2b to 2e. When $R_L \geq 1$, the plasma flows are no more deflected at $r = r_c$ but at $r = r_L$ by the particulate Lorentzian interaction (see Figs. 2c to fig 2e). In such a situation, no clear bow shock wave is formed upstream of the magnetic dipole, as seen in Fig. 3b.

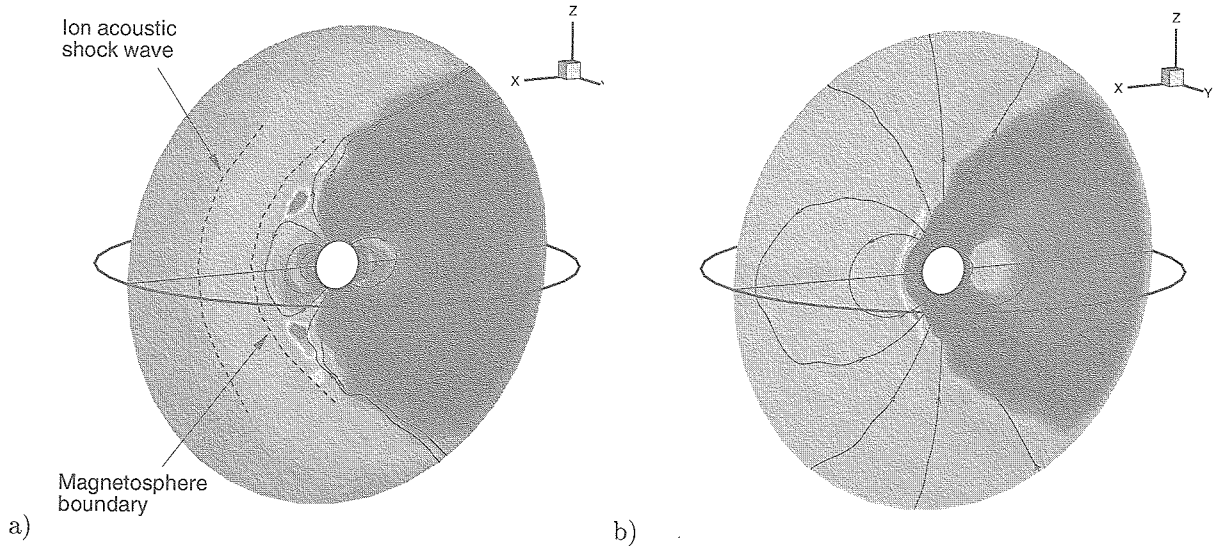

Fig 3: Ion number density distribution computed for a) Case 1 (R_L = 0.100) and b) Case 5 (R_L=10.0).

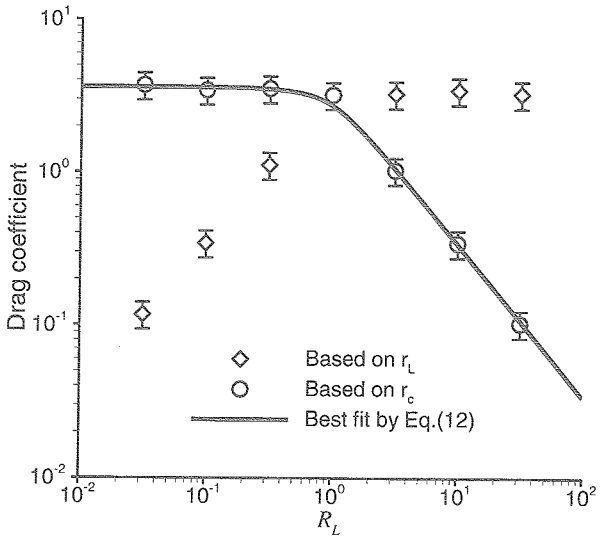

Fig 4: Variation of drag coefficients based on r_c and r_L along with R_L.

Drag force generated on the magnetic dipole, F_D, was computed from a change in the total kinetic momentum of inflowing and outflowing sample particles by taking an ensemble average after the flow and the magnetic field converged to a quasi-steady state. The drag coefficient, C_D, was computed using the drag force obtained above by

$$C_D = \frac{F_D}{\rho V_i^2 S/2} \tag{11}$$

where ρ is the mass density of the solar wind and S is the referential cross section. Two referential cross sections, $S_c \equiv \pi r_c^2$ and $S_L \equiv \pi r_L^2$ based on the magneto-hydrodynamic and the particulate interaction respectively, were used. The results are plotted against R_L in Fig.4.

The drag coefficient based on r_c is estimated to be 3.6±0.7 and independent of R_L when the magneto-

hydrodynamic interaction is dominant, or $R_L < 1$. However, the drag coefficient decreases along with an increase in R_L as the particulate Lorentzian interaction becomes superior to the magnet-hydrodynamic interaction, or $R_L \geq 1$. Contrary to this, the drag coefficient based on r_L is estimated to be 3.4 ± 0.7 regardless of R_L when the particulate Lorentzian interaction is dominant ($R_L \geq 1$), and decreases with R_L when the magnet-hydrodynamic interaction is dominant ($R_L < 1$). That is, the representative cross section of the dipole magnetic sail switches from S_c to S_L at $R_L = 1$. For above reasons, the non-dimensional parameter R_L is considered to be a measure of particulate effects on magneto-hydrodynamic interaction between the solar wind and the magnetic field generated by a magnetic dipole.

An approximate formula of the drag coefficient is given below for the purpose of quick estimation. The drag coefficient based on r_c is given as a function of R_L by

$$C_D = \begin{cases} 3.6\exp(-0.28R_L^2) & \text{for } R_L < 1 \\ \dfrac{3.4}{R_L}\exp\left(-\dfrac{0.22}{R_L^2}\right) & \text{for } R_L \geq 1 \end{cases} \tag{12}$$

In interaction between the solar sail and the magnetic dipole, R_H is related to r_c by

$$R_L = 1.02 \times 10^5 / r_c \tag{13}$$

As illustrated in Fig.4, good agreement is obtained between the drag coefficients calculated by Eq.(12) and obtained by the hybrid PIC computation.

The drag coefficient based on r_c is plotted against r_c in Fig.5, using Eqs. (12) and (13). The drag coefficient is found to decrease to 0.5 at r_c=15 km, and to 0.1 at r_c = 3 km approximately. Since the relation between r_c and r_L is based on the magnetic field generated by a magnetic dipole, in which the magnetic flux density decreases in proportion to r^{-3}, Eq. (12) may fail when other type of the magnetic field, such as the two dimensional induction coil and the inflated magnetoplasma sail, is used.

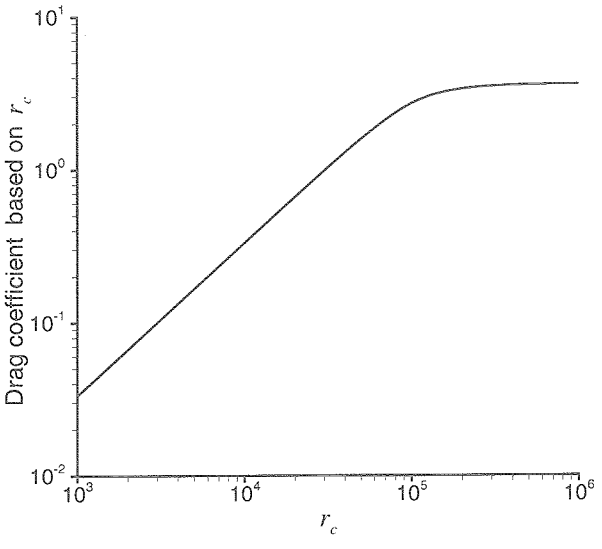

Fig 5: Variation of drag coefficients based on r_c along with r_c.

Conclusion

Numerical simulations of electromagnetic interaction between the solar wind and the magnetic dipole were made by using the hybrid PIC method for flows in which the finite Larmor-radius effect becomes significant. The drag coefficients of the magnetic dipole with respect to the solar wind were obtained in a wide range of magnetic sail dimension. The results show that electromagnetic interaction can be divided into two types according to the ratio of ion Larmor radius to the characteristic length of the initial magnetic field, R_L: the magneto-hydrodynamic interaction for $R_L < 1$ and the particulate Lorentzian interaction for $R_L \geq 1$.

The drag coefficient based on r_c is found to decrease as the finite Larmor-radius effect becomes significant, while that based on r_L is independent of R_L for $R_L > 1$. This suggests that the representative interaction radius of the magnetic dipole is given by r_c for $R_L < 1$ and by r_L for $R_L > 1$. An approximate formula describing the drag coefficient in a wide range of r_c is developed from the drag forces obtained by the PIC analysis. Using this formula, the drag coefficient is estimated to decrease to 0.5 at $r_c = 15$ km, and to 0.1 at $r_c = 3$ km approximately.

Refarences

[1] Winglee, R.M., Slough, J., Ziemba, T., and Goodson, A., "Mini-magnetospheric Plasma Propulsion: Tapping the energy of the solar wind for spacecraft propulsion," *J. Geophys. Res.*, **105**(20), 833 (2000).

[2] Winglee, R.M., Slough, J., Ziemba, T., and Goodson, A., "Mini-Magnetospheric Plasma Propulsion: High Speed Propulsion Sailing the Solar Wind," *in Space Technology and Applications International Forum-2000,* edited by El-Genk, M.S., CP504, AIP Press, 962 (2000).

[3] Winglee, R.M., Slough, J., Ziemba, T., Euripides, P., and Gallagher, D., "Laboratory testing of mini-magnetospheric plasma propulsion prototype," *in Space Technology and Applications International Forum-2001,* edited by El-Genk, M.S., CP552, AIP Press, 407 (2001).

[4] Yamakawa, H., Ogawa, H., Fujita, K., Nonaka, S., Sawai, S., Kuninaka, H., Funaki, I., Otsu, H., and Nakayama, Y., "Planetary Exploration by Magneto Plasma Sail," *J. Japan Society for Aeronautical and Space Science,* 52(603) 148 (2004).

[5] Yamakawa, H., "A Guidance Strategy for the Radially Accelerated Trajectory," AAS Paper 03-521, *AAS/AIAA Astrodynamics Spacialist Conference*, Montana, USA, (2003).

[6] Funaki, I., Asahi, R., Fujita, K., Yamakawa, H., Ogawa, H., Nonaka, S., Otsu, H., Sawai, S., and Kuninaka, H., "Thrust Production Mechanism of a Magnetoplasma Sail," AIAA Paper 2003-4292, *34th AIAA Plasma Dynamics and Lasers Conference*, Orlando, USA, (2003).

[7] Asahi, R., Funaki, I., Minami, T., Yamakawa, H., Fujita, K., Ogawa, H., "Thrust Production Mechanism of a Magnetoplasma Sail," Paper 2H9, *47th Symposium on Space Science and Technology*, Niigata, Japan, Nov. (2003).

[8] Nishida, H., Ogawa, H., and Inatani, Y., "MHD Analysis of Thrust on Magnetic Sail," ISTS 2004-s-30, *24th International Symposium of Space Technology and Science*, Miyazaki, Japan (2004).

[9] Fujita, K., Funaki, I., Ogawa, H., and Yamakawa, Y., "Thrust Production Analysis of Sub-scale Magnetoplasma Sail Using Particles Method," ISTS 2004-o-3-07v, 24th *International Symposium of Space Technology and Science*, Miyazaki, Japan (2004).

[10] Buchner, J., Dum., C.T., and Scholer, M., *Space Plasma Simulation,* Springer-Verlag, New York, (2003).

[11] Fujita, K., Inatani, Y., and Hiraki, K., "Attitude Stability of Blunt-Body Capsules in Hypersonic Rarefied Regime," *Journal of Spacecraft and Rockets,* 41(6) 925 (2004).